The structures of caspases-1, -3, -7 and -8 reveal the basis for substrate and inhibitor selectivity

Yunyi Wei, Ted Fox, Steve P Chambers, JoAnne Sintchak, Joyce T Coll, Julian MC Golec, Lora Swenson, Keith P Wilson and Paul S Charifson

Background: Peptide inhibitors of caspases have helped define the role of these cysteine proteases in biology. Structural and biochemical characterization of the caspase enzymes may contribute to the development of new drugs for the treatment of caspase-mediated inflammation and apoptosis.

Results: The crystal structure of the previously unpublished caspase-7 (Csp7; 2.35 Å) bound to the reversible tetrapeptide aldehyde inhibitor acetyl-Asp–Glu–Val–Asp-CHO is compared with crystal structures of caspases-1 (2.3 Å), -3 (2.2 Å), and -8 (2.65 Å) bound to the same inhibitor. Csp7 is a close homolog of caspase-3 (Csp3), and these two caspases possess some quarternary structural characteristics that support their unique role among the caspase family. However, although Csp3 and Csp7 are quite similar overall, they were found to have a significantly different substitution pattern of amino acids in and around the S4-binding site.

Conclusions: These structures span all three caspase subgroups, and provide a basis for inferring substrate and inhibitor binding, as well as selectivity for the entire caspase family. This information will influence the design of selective caspase inhibitors to further elucidate the role of caspases in biology and hopefully lead to the design of therapeutic agents to treat caspase-mediated diseases, such as rheumatoid arthritis, certain neurogenerative diseases and stroke.

Address: Vertex Pharmaceuticals, 130 Waverly Street, Cambridge, MA 02139-4242, USA.

Correspondence: Paul S Charifson
E-mail: paulc@vpharm.com

Key words: caspases, inhibitor design structure, selectivity

Received: **22 November 1999**
Revisions requested: **13 January 2000**
Revisions received: **28 February 2000**
Accepted: **16 March 2000**

Published: **30 May 2000**

Chemistry & Biology 2000, **7**:423–432

1074-5521/00/$ – see front matter

Introduction

The caspase (Csp) enzymes are receiving increasing attention as targets for the design of new drugs, and reviews of this family of cysteine proteases are abundant [1–6]. The Csp family can be divided into three subfamilies, based on their predominant functional roles and their substrate specificities [5,7]. The family members most closely related to Csp1 (also known as interleukin-1β converting enzyme [ICE]) are mainly involved in pro-inflammatory events. Inhibitors of these enzymes have potential as anti-inflammatory drugs for use in diseases such as rheumatoid arthritis [8]. The remaining caspases are of central importance in the pathways controlling apoptosis. Inhibitors of these enzymes may lead to compounds useful for the treatment of an array of diseases, such as stroke and neurodegeneration, for which there are few effective therapies. Peptidic caspase inhibitors have already shown efficacy in models of myocardial infarction [9], stroke [10,11], traumatic brain injury, [12] and fulminant liver disease [13].

The first orally active inhibitor of Csp1, VX740, has been reported recently [14]. The design of VX740 started with the crystal structure of the complex of Csp1 with the tetrapeptide aldehyde acetyl-Tyr–Val–Ala–Asp-CHO (Ac-YVAD-CHO). In this work, we report the crystallographic complexes of Csp1, Csp3, Csp8, and the first reported structure of Csp7, all bound to the same tetrapeptide aldehyde inhibitor, acetyl-Asp–Glu–Val–Asp-CHO (Ac-DEVD-CHO). Examination of this new data, coupled with that from previously published complexes of Csp1 [15–18], Csp3 [19,20] and Csp8 [21,22] gives invaluable information for the design of inhibitors of all three Csp families.

Results and discussion

Crystallography

The model quality of all four structures was assessed using PROCHECK [23] and the crystallographic statistics are given in Table 1.

The Csp7–Ac-DEVD-CHO complex is similar to the Csp3–Ac-DEVD-CHO complex

The refined model of Csp7 contains a complete catalytic unit comprising two p20–p10 heterodimers. The p20 and p10 polypeptide chains are composed of residues 57–196 and 212–302, respectively. The two interdigitating heterodimers associate to form a tetramer of globular shape. A ribbon stereo diagram of the Csp7 complex is illustrated in Figure 1. As expected, the overall fold of Csp7 is very similar to that of Csp1, Csp3 and Csp8. All four subunits contribute to a total of 12 strands comprising the central β sheet. This forms the core of the enzyme,

Table 1

Crystallographic data and refinement statistics.

	Csp1	Csp3	Csp7	Csp8
X-ray experiments				
Temperature (K)	266	270	100	100
X-ray radiation	Rotating anode	Rotating anode	$\chi=5$ at BNL‡	BNL
Wavelength (Å)	1.5418	1.5418	1.10	1.09
Space group	$P4_32_12$	$P2_12_12_1$	P_3221	$C222_1$
a(Å)	62.45	89.46	88.18	62.12
b(Å)	62.45	97.33	88.18	344.33
c(Å)	162.36	70.09	186.23	190.99
α(°)	90	90.0	90	90
β(°)	90	90.0	90	90
γ(°)	90	90.0	120	90
No of p20/p10 in asym. unit	1	2	2	6
Recording apparatus	R_{axis} IIC	R_{axis} IIC	CCD 2X2K	CCD 2X2K
Resolution (Å)	2.5	2.2	2.35	2.65
Total observation	48936	63425	139781	189632
Unique reflection	13468	12532	34359	53183
Completeness (%)	93	92	96.6	88.2
R_{sym}* (%)	6.5	7.8	8.3	5.5
Structure solution				
Methods	See [16]	MR	MR	MR
Search model	See [16]	PolyAla of Csp1	PolyAla of Csp3	PolyAla of Csp3
Resolution range (Å)	See [16]	8.0–2.8	16.0–4.0	16.0–4.0
Software	See [16]	AmoRe	AmoRe	AmoRe
R-factor (%)	See [16]	45.1	41.0	34.7
Correlation coefficient Factor	See [16]	54.6	61.0	72.5
Refinement				
Resolution range (Å)	7.5–2.5	8.0–2.2	7.5–2.35	20.0–2.65
Sigma cut off (σ)	2.5	3.0	2.5	2.5
Programs	X-PLOR	X-PLOR	X-PLOR	X-PLOR
No of reflections	14,658	24,890	33,303	48,348
R-factor† (%)	23.1	18.9	18.5	21.9
Free R-factor† (%)	28.2	24.7	26.3	28.6
Stereochemical parameters				
Rms bond distance (Å)	0.011	0.009	0.009	0.006
Rms bond angle (°)	2.3	1.9	1.8	1.7
Rms dihedral angle (°)	24.1	23.6	23.4	23.4
Nonglycine residues in the regions of most favored (%)	90.0	89.3	89.0	86.3
Additional allowed (%)	9.5	9.0	10.5	13.7
Generously allowed (%)	0.5	0.7	0.5	0.0
Disallowed (%)	0	0	0	0.0

*$R_{sym} = \Sigma|I_i - \langle I\rangle|/\Sigma I_i$, where I_i and $\langle I\rangle$ are the intensities for the *i*th observation and mean of the reflection, respectively.
†R-factor $= \Sigma|F_{obs} - F_{cal}|/\Sigma|F_{obs}|$, where F_{obs} and F_{cal} are observed and calculated model structure factors. Free R-factor was calculated with 5% of each data set not used in the refinement. ‡ Brookhaven National Laboratories.

which is flanked by ten α helixes approximately parallel to the β strands. In particular, the β-sheet structure of the p20 domain, which contains the catalytic His285 and Cys186 residues, has a crossing-over –1X, +2X, +1X linking topology according to Richardson's definition [24]. This motif has been widely observed in serine hydrolases, most notably the α/β hydrolase superfamily [25].

Among the three subfamilies of caspases, Csp7 belongs to the second group that includes Csp2 and Csp3. Aside from the differences that exist in the propeptide and linker regions, Csp7 is structurally and functionally very similar to Csp3. In fact, Csp7 and Csp3 can be superimposed without any amino acid deletions or insertions along the polypeptide chains (Figure 2a) with a root mean square (RMS) deviation of 0.37 Å for backbone Cα atoms. Sequence alignment and Cα atom superpositioning of Csp1, Csp3, Csp7 and Csp8 spanning all three caspase subfamilies (Figures 2a and 3) demonstrated that the main differences between their folds are in three regions. These differences occur in the two loops on the prime side and a third loop proximal to the S4 binding site (Figure 2a).

Similar to Csp3, Csp7 also has a single-residue deletion within the strand C290–M294 (Figure 3), which pairs with its symmetry-related equivalent forming the tetrameric

Figure 1

Stereoview of Csp7 tetrameric assembly made using RIBBONS [46]. The p20, p10 and their symmetry related equivalents, p20′ and p10′, are shown in green, yellow, blue and violet, respectively. The ball-and-stick model shown in cyan represents the Ac-DEVD-CHO inhibitor.

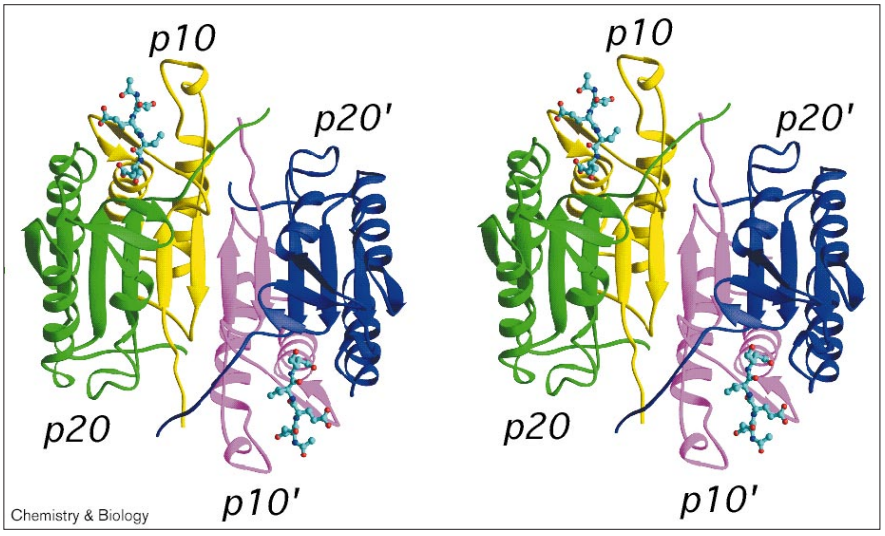

assembly of the enzyme. In Csp1 and other caspases of group 1, there is an arginine residue (R391 in Csp1) which causes a bulge in the β strand and consequently induces a rotation of one heterodimer relative to the other. In Csp3 [20] and Csp7, the two dimeric subunits are significantly less twisted. The combination of this single deletion and greater hydrophobic nature of this strand in Csp3 and Csp7 has not only changed the quaternary structures of these enzymes but also reshaped the central cavity formed at the interface of the two heterodimers. The central cavity of the Csp7 tetramer was occupied by 24 water molecules. As this central cavity is adjacent to the prime side of the substrate binding site, it may not effect directly substrate binding to Csp3 and Csp7. However, the variation in the central cavity among caspases might be an important determinant of macromolecular substrate recognition in the apoptosis cascade.

Binding of Ac-DEVD–CHO to caspases from all three subfamilies

The four caspases included in this study span three different functional and phylogenetic groups of caspases, and each exhibits subtle differences in the way they bind Ac-DEVD-CHO. The peptide inhibitor has adopted an

Figure 2

Secondary structural elements of Csp1, Csp3, Csp7 and Csp8. **(a)** Conserved fold for superimposed Csp1 (cyan), Csp3 (violet), Csp7 (yellow), Csp8 (green) with covalently bound tetrapeptide inhibitor, Ac-DEVD-CHO. **(b)** Superimposed S4 loops for Csp1 (378–386), Csp3 (244–262), Csp7 (270–288) and Csp8 (451–463). **(c)** Prime side helix–turn–helix insertion in Csp8 ranging from residues 245–253 proximal to superimposed insertion loop of Csp1 (Figure 2c: residues 249–254). Panels (b) and (c) have been rotated slightly relative to (a).

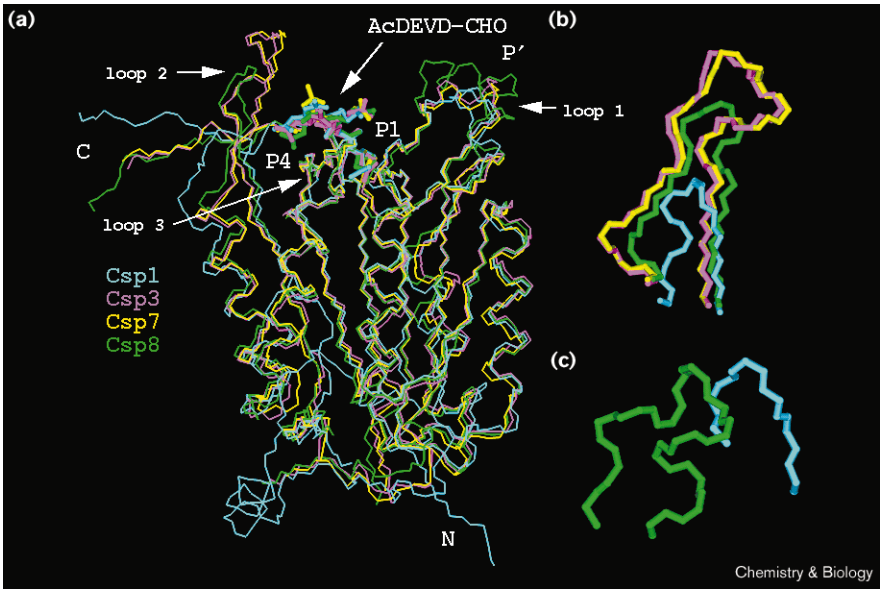

Figure 3

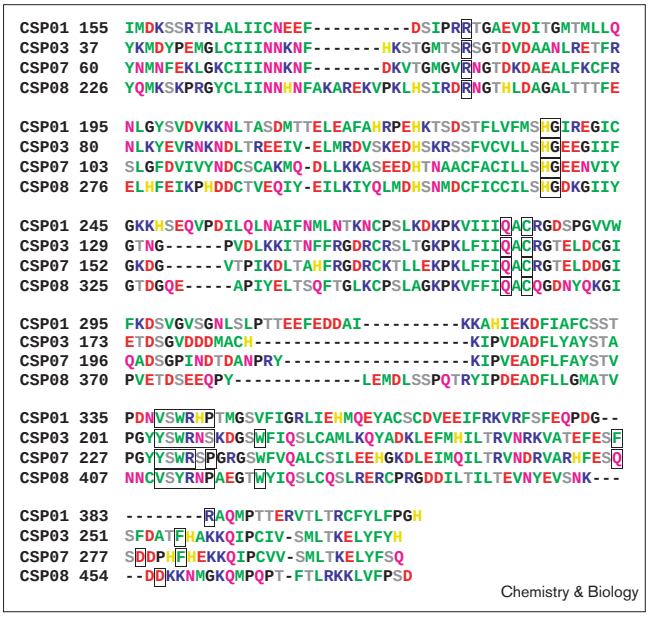

Sequence alignment of Csp1, Csp3, Csp7 and Csp8. The alignment was heavily biased upon the superposition of conserved secondary structural elements and active site residues of Csp1, Csp3, Csp7 and Csp8. The alignment was performed with the MVP program [47] and then adjusted manually. Boxed residues denote direct or water-mediated interactions with Ac-DEVD-CHO as shown in Figure 4. Amino acid color coding is as follows: green, hydrophobic; purple, basic; orange, acidic; yellow, histidine; black, proline, glycine; gray, serine and threonine; pink, asparagine and/or glutamine.

extended conformation in all four complexes. Besides the fact that the catalytic dyad and two residues anchoring the aspartate residue in the P1 position are from the p20 domain, most of the intimate contacts are between the tetrapeptide and the groups from the p10 subunit. Although there are differences in some of the amino acid residues from each caspase that contribute to binding Ac-DEVD-CHO, the overall conformation of the inhibitor is highly conserved. A schematic comparing Ac-DEVD-CHO binding to Csp1, Csp3, Csp7 and Csp8 is shown in Figure 4, whereas Figure 5 shows the surface features of the respective binding sites. We will now consider the similarities and differences with which each of the four caspases binds each of the tetrapeptide P1–P4 residues.

At the P1 site, all four of the complexes show that the inhibitor is covalently bound to the nucleophilic cysteine residue in the active site (Figure 4), although binding to the classic oxyanion hole was not observed. In each case, the thiohemiacetal oxygen resulting from nucleophilic thiol attack on the aldehyde carbonyl forms a hydrogen bond with the adjacent histidine that comprises the enzyme's cysteine–histidine dyad. In addition, the thiohemiacetal oxygen in all four complexes makes hydrogen bonds of varying strength to the nucleophilic cysteine backbone nitrogen and conserved glycine backbone nitrogen. Previous work [15,20] has shown that some irreversible inhibitors exhibit classic oxyanion hole-binding to Csp1 and Csp3. The other interactions at P1 are also strikingly conserved among the four structures. In every case, there are charge–charge interactions between the P1 aspartate sidechain and two arginine residues, as well as a hydrogen bond with a conserved glutamine. Figure 5 shows the conserved nature of this overwhelmingly electropositive site and the buried nature of the P1 aspartate. Additionally, each complex retains a hydrogen bond between the P1 backbone nitrogen and the backbone carbonyl of a conserved serine.

For the P2 valine of Ac-DEVD-CHO, the overall nature of the hydrophobic interaction is conserved, but there are subtle differences in the $\chi 1$ value for the valine sidechain, depending on the residues comprising the S2 pocket. Interestingly, Csp3 and Csp7 possess an extra residue (phenylalanine) which contributes to the S2 site and is also part of the S4 loop. Csp8 also possesses an aromatic residue (Tyr365) at roughly the same spatial position as Phe256 of Csp3 and Phe282 of Csp7, but this tyrosine residue is part of an extended strand near the carboxyl terminus of the p20 subunit. Residues corresponding to Tyr365 of Csp8 are Pro290 (Csp1), Leu168 (Csp3), and Leu191 (Csp7). None of these contribute directly to the S2 site in the corresponding complexes with Ac-DEVD-CHO.

The P3 glutamic acid of the tetrapeptide inhibitor, makes at least one charge–charge interaction with a conserved arginine in all four caspase complexes (Figure 4). Additionally, the P3 backbone nitrogen and carbonyl oxygen of the P3 glutamic acid make strong hydrogen bonds with the respective backbone carbonyl oxygen and nitrogen of the same arginine involved in the surface charge interaction. Csp8 also has an additional charge–charge interaction from a second arginine residue (Arg258), which follows the helix–turn–helix insertion loop. This is in agreement with recent findings in which a similar peptide inhibitor is complexed with Csp8 [21]. Analysis of Figure 5 shows that the P3 glutamic acid of the Ac-DEVD-CHO inhibitor is oriented towards this second (i.e. Arg258) arginine residue on the protein surface of Csp8. A crystallographic water molecule is observed binding to the conserved arginine for Csp3, Csp7 and Csp8.

The differences in size of the S4 loop among the four caspases in this study are striking. These loops involve the following residues: Csp1 (378–386); Csp3 (244–262), Csp7 (270–288); and Csp8 (451–463). Figure 2b illustrates that this loop is largest for Csp3 and Csp7. Despite the fact that this loop is identical in length for these two closely related caspases, they are only 63% identical in composition. The same loop is shorter for Csp8 and shorter still for Csp1. In each case, there is an interaction between the P4

Figure 4

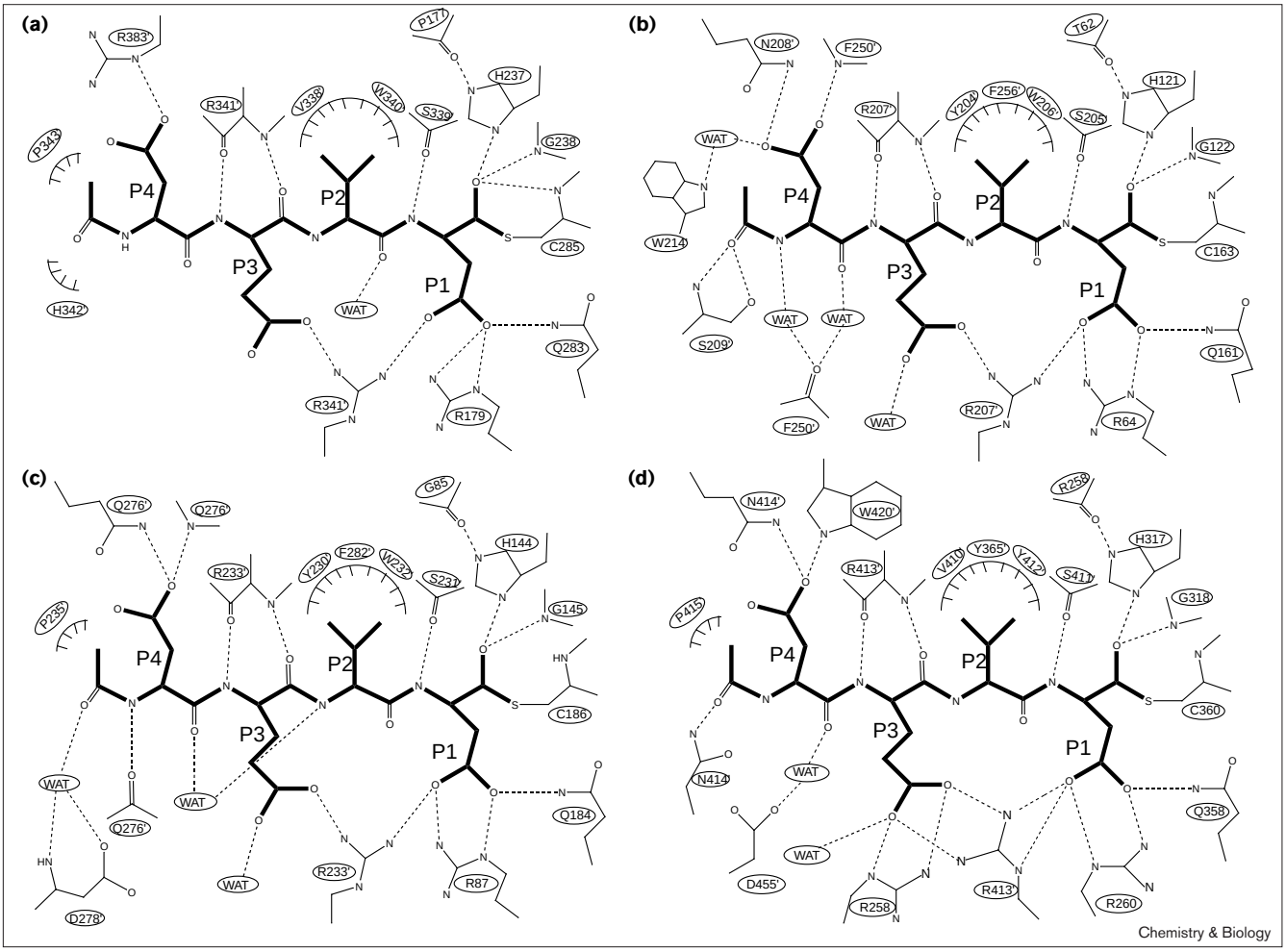

Schematic showing hydrogen bonding and van der Waals interactions of covalently bound Ac-DEVD–thiohemiacetal with binding-site residues of **(a)** Csp1, **(b)** Csp3, **(c)** Csp7 and **(d)** Csp8. Wat, water molecule.

aspartic acid of the Ac-DEVD-CHO inhibitor and a residue in this loop.

The major differences for the binding of Ac-DEVD-CHO to Csp1, Csp3, Csp7 and Csp8 occur at the P4 aspartic acid and the acetylated amino terminus of the tetrapeptide. All of the caspases included in this study involve either direct or indirect binding by the S4 loop. Figure 4 shows that Csp1 interacts with the P4 aspartic sidechain directly through an interaction with Arg383. Csp3 interacts via the backbone nitrogen of Phe250 and the sidechain of Asn208. In this case, there is also an interaction of the P4 aspartic acid with Trp214 through a water-mediated hydrogen bond. Additionally, the P4 backbone nitrogen and carbonyl oxygen forms hydrogen bonds with two different water molecules, both of which form hydrogen bonds with the carbonyl group of Phe250. Csp7 binds the P4 aspartic acid through both backbone and sidechain involvement of Gln276. The P4 backbone nitrogen forms an additional hydrogen bond with the backbone carbonyl of Gln276 while the P4 backbone carbonyl oxygen forms a hydrogen bond to the same crystallographic water molecule involved in another hydrogen bond with the P2 backbone nitrogen. It is interesting to note that, although the Csp3 and Csp7 sequences share 57% and 67% similarity (Figure 3), there are significant differences in and around the S4-binding region. The replacement of Csp3 residues (Asn208, Ser209, Asp211, Phe250, Phe252, Thr255, and Ala258 by their respective Csp7 residues (Ser234, Pro235, Arg237, Gln276, Asp278, His281 and Glu284) has changed the chemical content (Figure 5) in the S4-binding region to be more hydrophilic.

Csp8 interacts directly with the P4 aspartate residue via the sidechain nitrogens of Asn414 and Trp420 that are not part of the S4 loop. However, the P4 aspartate

Figure 5

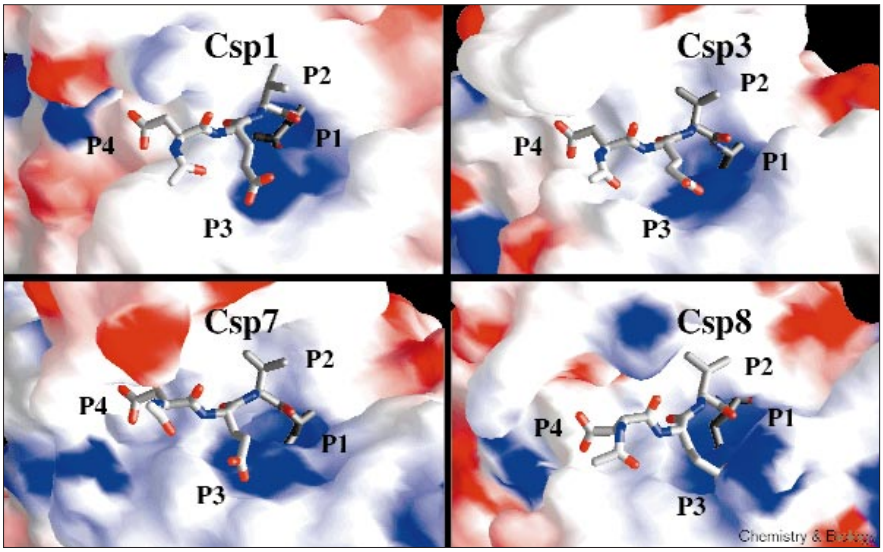

Electrostatic potential mapped onto molecular surface for binding-site residues of Csp1, Csp3, Csp7 and Csp8. Blue depicts areas of positive electrostatic potential, red depicts areas of negative electrostatic potential and white represents areas of neutral electrostatic potential. The molecular surface and electrostatic potential were calculated using GRASP [48].

carbonyl oxygen interacts with Asp455 via a water-mediated hydrogen bond.

The *N*-acetyl P4 capping group also exhibits differences in hydrogen bonding and hydrophobic interactions. Csp1, Csp7 and Csp8 all make a hydrophobic interaction between the *N*-acetyl terminal methyl group and a proline (Figure 4). Csp3 lacks this hydrophobic interaction, but makes two hydrogen bonds with Ser209, one involving the Ser209 backbone nitrogen, the other with the Ser209 sidechain. Csp7 forms a water-mediated hydrogen bond with both the backbone nitrogen and sidechain of Asp278. For Csp8, the *N*-acetyl carbonyl oxygen forms a hydrogen bond to the sidechain of Asn414. No hydrogen bond is observed between Csp1 and the *N*-acetyl group. One final observation regarding differences in binding the *N*-acetyl group occurs between Csp3 and the other three caspases included in this study. As mentioned above, there are two strong hydrogen bonds between the *N*-acetyl group and Ser209 of Csp3. In Csp1, Csp7 and Csp8, however, the residue corresponding to Ser209 is a proline; any hydrogen-bonding interactions of the *N*-acetyl group involves different residues. Owing to the inability of the proline ring to form hydrogen bonds, the P4 *N*-acetyl group is translated ~2.5 Å. Figure 6 illustrates this shift between Csp3 and Csp7. These are members of the same caspase subfamily.

The differences in hydrogen bonding of the P4 and *N*-acetyl groups with the associated caspase residues results in a variable width of the S4 site with Csp8 having the widest S4 site, followed by Csp1 (Figure 5); Csp3 and Csp7 have a narrower S4 site. For Csp3 and Csp7, the reduced width in the S4 site can be directly linked to the greater extent of the hydrogen-bond network between this portion of the tetrapeptide and the S4 site which serves to 'pull' the walls of the S4 pocket towards the P4 group. On this point, the electrostatic potential surfaces illustrated in Figure 5 are informative. The surface potential of Csp7 is unique because it is the only caspase of the four studied that has an unpaired basic residue (Arg237) near the P4 aspartic acid. Csp1 and Csp8 also have basic residues that contribute to the electropositive portion of the surface potential in this region, but they also have counterbalancing negative charges near by. Csp3 has a neutral S4 region. These observations suggest that, in terms of structure and associated surface potential, there should be no absolute requirement for a negatively charged group at P4.

On the prime side, Csp8 differs from the others by the presence of a helix–turn–helix insertion ranging from residues 245–253 (Figure 2c). This agrees with the recently reported Csp8 structures expressed in *Escherichia coli* [21,22] that also possess some helical content to this insertion loop. An analysis of a sequence alignment derived from superposition of the four caspase structures (Figure 3) suggests this insertion to be unique to Csp8. Three of the lysines in this region (Lys246, Lys250, Lys253) were mutated to arginine in order to obtain diffraction quality crystals. A comparison of wild-type and the mutant form of Csp8 used to determine the crystal structure showed that both enzymes appear to be indistinguishable, yielding a k_{cat}/K_m of $1 \times 10^5\ M^{-1}s^{-1}$ for Ac-DEVD–aminomethylcoumarin (Ac-DEVD–AMC) hydrolysis. Two of these mutated arginines are stabilized by a salt bridge with nearby glutamic residues (Arg250 with Glu249, Arg253 with Glu330, Arg246 with a glutamic acid from a symmetry-related neighbor. None of these mutated residues is oriented in the prime side region,

Figure 6

A stereoview diagram showing the superposition of Csp3 (orange) with Csp7 (cyan) generated by RIBBONS. The *N*-acetyl group of the tetrapeptide inhibitor, Ac-DEVD-CHO, bound to Csp7 (green) is translated ~2.5 Å relative to that in Csp3 (dark brown) due to the substitution of proline (235) for serine at the same position of the P4-binding site.

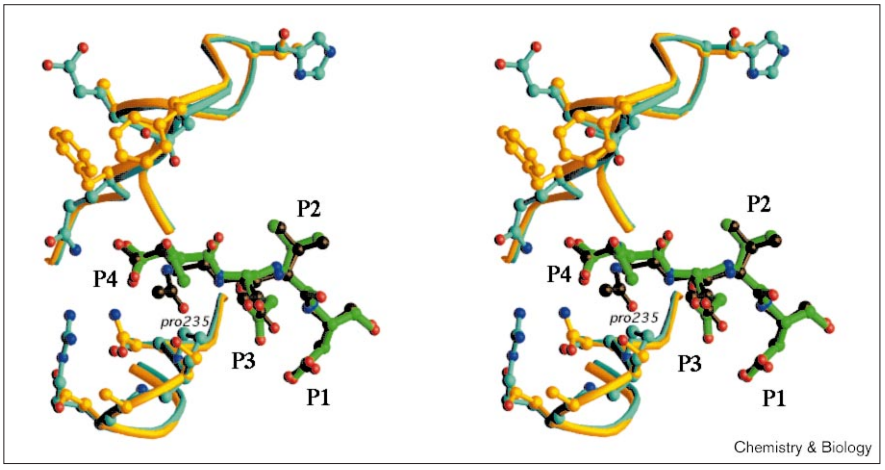

nor are they in close proximity to the tetrapeptide inhibitor. Leu254, from this helix–turn–helix insertion, appears to point inward towards the prime side region. The spatial position of the helix–turn–helix insertion for Csp8 most closely resembles a short insertion loop of Csp1 (Figure 2c: residues 249–254) which is conserved among the members of the Csp1 family.

Structural insights and binding specificity

On the basis of positional scanning of a combinatorial substrate library, Thornberry *et al.* [26] were able to determine the optimal tetrapeptide substrate sequences for ten human caspases. In this study, a cleavable Asp-AMC was held constant at P1 and the amino acids at P2 through P4 were varied. They found that group I (Csp1, Csp4 and Csp5) caspases loosely preferred the sequence WEHD, while group II (Csp2, Csp3 and Csp7) caspases strongly preferred the motif DEXD. Group III (Csp6, Csp8, Csp9 and Csp10) caspases preferred the motif (L/V)EXD. This information was subsequently used to design and investigate tetrapeptide aldehyde inhibitors [7]. Some traditional reversible inhibitors and irreversible inhibitors such as Z–VAD–FMK were also included in the study.

Reported K_i values (nM) from reference sequences [7] for Ac-DEVD–CHO against Csp1, Csp3, Csp7 and Csp8, respectively, are as follows: 18 nM, 0.23 nM, 1.6 nM and 0.92 nM. Although this tetrapeptide inhibitor is most potent against group II and III caspases, it is the only reported tetrapeptide aldehyde that significantly inhibits representatives from all three groups of caspases. The fact that all caspases considered here can accommodate a valine at P2 attests to the general tolerability of branched amino acids at this position. However, branched amino acids at P2 tend to produce less optimal substrates against Csp1, Csp4 and Csp5 [26] and are typically not present in the best inhibitors for Group I caspases. In general, large groups are tolerated as both substrates and inhibitors for all three caspase subfamilies and even though tetra peptide substrates containing tryptophan, phenylalanine, and tyrosine at P2 are suboptimal, histidine-containing tetrapeptide substrates were generally good against group I and III caspases [26]. Additionally, in a previous crystallographic study, a nonpeptidic pyridone aldehyde inhibitor containing a large 6-benzyl substituent on the pyridone ring was found to place the phenyl ring of the benzyl group over the S2 site in Csp1 [27].

The optimal residue identified by the combinatorial tetrapeptide substrate library [26] at the P3 position for all three groups of caspases is glutamic acid. All four caspases in the present study make at least one charge–charge interaction with the P3 glutamic acid. The nature of this interaction involves an absolutely conserved arginine; however, this salt bridge is on the surface of the protein and is solvent exposed. In terms of substrate specificity, such an interaction might be optimal in terms of recognition and proper positioning of the peptide backbone, but would be expected to contribute minimally to the overall binding energetics [28]. This is illustrated by the inhibitor Ac-YVAD-CHO which shows good inhibitory potency against Csp1 and modest inhibitory potency against group III caspases. Although the surface charge–charge interaction(s) would be lost, the P3 valine would be expected to still make the required backbone hydrogen bonds and a potential hydrophobic interaction with a either a proline (Csp1, Csp7, Csp8) or the β carbon of serine (Csp3). The branched P3 valine would also serve to maintain the rigidity of the extended tetrapeptide inhibitor and could potentially improve cell potency due to one less formal charge on the molecule. A recent report of peptidomimetic caspase inhibitors shows reasonably potent inhibition of multiple caspases in a compound class that

would be incapable of making a charge–charge interaction with the conserved S3 arginine [29].

In terms of both substrate specificity and inhibitor selectivity, the P4 position offers the most variability. In general, both hydrophobic groups and the anionic aspartate are tolerated at the P4 position for both substrates and inhibitors. For group II and III caspases, a tryptophan rests at the bottom of the S4 pocket. For group I caspases, this same residue is a smaller hydrophobic amino acid (e.g. Val348 in Csp1). The binding of Ac-DEVD-CHO to Csp1 produces fewer total hydrogen bonds with S4 residues relative to the other caspases studied, and this allows for a wider S4 pocket. The combination of fewer hydrogen bonds and a neutral electrostatic potential in this portion of the binding site suggests that group I caspases could accommodate larger hydrophobic groups at S4, thereby providing an avenue to gain selectivity in the design of inhibitors. The combinatorial tetrapeptide substrate study [26] showed that WEHD was the optimal substrate for Csp1 and was also a good substrate for the other group I caspases, Csp4 and Csp5. However, leucine was roughly equal to tryptophan at P4 as a substrate for these two caspases. Group II caspases were shown to have a strong preference for substrates with aspartic acid at P4. As alluded to above, the replacement of hydrophobic residues in Csp3 by charged or hydrophilic residues in Csp7 might allow these two seemingly redundant caspases to act on different substrates in different cell types or cellular compartments [30,31] even though their *in vitro* substrate preferences are identical. Group III caspases prefer either valine or leucine at the P4 position. Interestingly, in terms of inhibitors, Ac-WEHD-CHO showed the most potent inhibition against Csp1, suggesting that the valine at the bottom of the S4 pocket leaves enough room for the P4 tryptophan to be accommodated [7]. Although Csp8 has a large tryptophan residue at the bottom of the S4 pocket, this portion of the binding site is fairly wide and can accommodate the P4 group of Ac-WEHD-CHO. Similar trends are observed for inhibitors containing tyrosine or benzyloxycarbonyl groups at P4. Additionally, the first selective Csp1 inhibitor to reach clinical trials, VX-740, possesses an isoquinoline group at P4. The X-ray crystallographic structure of this inhibitor clearly shows the P4 isoquinoline fitting snugly in the S4 pocket (Mullican *et al.*, unpublished observations). Thus, although it is possible to design selective Csp1 inhibitors by incorporation of large hydrophobic groups at P4, it is not clear that one can take advantage of the P4 position to design selective inhibitors of other caspases.

Significance

The caspase family has continued to evoke intense interest in the world of biology and biomedical research. Caspase inhibition has produced desired pharmacological effects in animal models for stroke, myocardial infarction, traumatic brain injury, liver disease and interleukin-1β-mediated inflammatory conditions. Biochemical studies further suggest the utility of caspase inhibitors in the treatment of various neurodegenerative diseases [32–37]. Despite this, much caspase biology remains to be uncovered, and it is still difficult to assess the relative contribution of individual caspases to effect specific cellular events without the benefit of specific inhibitors.

A better understanding of caspase structures spanning all of the caspase subfamilies provides the framework for the design of potent and selective inhibitors of individual caspases. These molecules will, in turn, help uncover the biology in this field and open the way for the use of caspase inhibitors in the treatment of relevant diseases.

It is hoped that the crystallographic complexes of Csp1, Csp3, Csp8 and the new structure of Csp7 bound to the same tetrapeptide aldehyde inhibitor, Ac-DEVD-CHO, presented here can contribute towards this goal.

Materials and methods

Expression and purification of Csp1, Csp3, Csp7 and Csp8

Recombinant human Csp1 was expressed in *E. coli* as an insoluble p32 protein spanning residues 120–404 of the p45 precursor [38]. The insoluble p32 protein was solubilized and purified under chaotropic conditions, then refolded and autoprocessed *in vitro*, producing the p20 and p10 active subunits. Details, including previous X-ray crystallographic analyses, have been described elsewhere [16,17].

Csp3 (residues 29–277) and Csp7 (residues 1–303) containing an amino-terminal His_6 affinity tag and thrombin-cleavable site were expressed in *E. coli* [39,40]. Both caspases were soluble and active as their p20–p10 subunits, yielding 0.05 mg/g and 1 mg/g cells of Csp3 and Csp7, respectively. For purification of either protein, cell paste was resuspended in 10 volumes of 50 mM HEPES buffer containing 10% (v/v) glycerol, 300 mM NaCl, 5 mM β-ME, 0.05% (w/v) β-OG, 25 mM imidazole, 0.1 mM PMSF, pH 8.0 at 4°C. Following mechanical disruption of the cells, the soluble fraction was harvested by centrifugation at 30,000 ×*g* for 30 min at 4°C. The supernatant was incubated batchwise overnight with 1 ml Ni-affinity resin (Qiagen, Valencia, CA) per 5–10 mg of expected Csp3 or Csp7. The resin was washed with 50 column-volumes of the extraction buffer, followed by 50 column-volumes of the extraction buffer adjusted to pH 7.0. Csp3 and Csp7 were eluted with 50 mM and 300 mM imidazole, respectively, in 50 mM HEPES, pH 7.0 containing 10% (v/v) glycerol, 100 mM NaCl, 5 mM β-mercaptoethanol (β-ME).

Recombinant Csp8 (residues 233–479) was expressed as an amino-terminal histidine-tagged fusion in High-five insect cells using a baculovirus expression vector system by conventional methods [41]. Crystallization of Csp8–Ac-DEVD-CHO was enhanced by three Lys→Arg point mutations (at residues 246, 250 and 253), and removal of Pro370 and Val371, which appeared absent from other caspases in sequence alignments. Csp8 was processed intracellularly and secreted into the media during expression. The cell culture media was centrifuged at 1600 ×*g* to remove cells, and the supernatant (~pH 6.4) adjusted to 50% (w/v) ammonium sulfate and stirred gently for 60 min on ice. After centrifugation at 54,000 ×*g* for 45 min at 4°C, the supernatant was decanted, 0.2 μm filtered and the ammonium sulfate concentration increased to 85% (w/v) and stirred for another 60 min on ice. Centrifugation at 54,000 ×*g* for 45 min at 4°C resulted in the pre-

cipitation of Csp8. Pellets were resuspended in 2% of the starting volume of the media using 100 mM HEPES, pH 8.0, containing 100 mM NaCl, 10% glycerol (v/v) and 5 mM β-ME. The solution was incubated with 1 ml Talon affinity resin (Clontech, Palo Alto, CA) per 5–10 mg expected Csp8 and gently mixed overnight at 4°C. The resin washed with 150 column volumes of 20 mM HEPES, pH 7.0, containing 100 mM NaCl, 10% glycerol (v/v) and 5 mM β-ME. A second wash of 50 column volumes was performed using the same buffer, with 25 mM imidazole. Csp8 was eluted with wash buffer adjusted to 350 mM imidazole.

Characterization of triple mutant Csp8

Wild-type and mutant Csp8 enzymes were characterized using the fluorogenic substrate Ac-DEVD–AMC (Alexis Biochemicals, San Diego, CA). The concentrations of active enzyme were determined by active-site titration with Ac-DEVD-CHO (Peptides International, Lousiville, KY). All assays were performed in 100 mM HEPES, pH 8, containing 100 mM NaCl, 5 mM DTT and 0.1% (w/v) CHAPS at 37°C using a 96-well Fmax plate reader (Molecular Devices, Sunnyvale, CA). The Ac-DEVD-AMC substrate concentration was varied between 2 and 100 μM and the reaction was initiated by addition of 2 nM enzyme. Enzyme kinetic data were analyzed by nonlinear regression in the program EZ-Fit (Perrella Scientific, Amherst, NH).

Preparation of Csp–Ac-DEVD-CHO crystallographic samples

Details of protein purification and crystallization of the Csp1–Ac-DEVD-CHO complex has been reported [17]. Metal affinity purified Csp3, Csp7 or Csp8 were inhibited by addition of a two-fold molar excess of Ac-DEVD-CHO (Peptides International). The amino-terminal His_6 tag was then removed from Csp3, Csp7 or Csp8 by thrombin cleavage (20 units of thrombin per mg caspase) at 37°C for 60 min. Thrombin was removed by a 5 min incubation with 100 μl of benzamidine sepharose. The free His_6 tag and aggregated caspase were removed by size-exclusion chromatography using a column (60 × 1.5 cm) packed with Superdex-75 resin (Pharmacia, Uppsala, Sweden). The column was equilibrated at 4°C in 20 mM HEPES, pH 7.0, containing 10% glycerol (v/v), 100 mM NaCl, 5 mM β-ME at a flow rate of 1 ml min^{-1}. Light-scattering (PD-2000, Precision Detectors, Franklin, MA) analyses during size-exclusion chromatography identified aggregated protein, which was excluded from the pooled fractions. Csp1–Ac-DEVD-CHO was purified on the same size-exclusion column except 50 mM citrate, pH 6.5, containing 2 mM DTT buffer was used. After size-exclusion, equimolar Ac-DEVD-CHO was added prior to concentration of the Csp–Ac-DEVD-CHO co-complexes for crystallization. All protein samples were stored at −70°C.

Crystals of inhibited Csp3 were grown by vapor diffusion and macroseeding. Thousands of microcrystals were initially obtained in 12 h when protein (4.6 mg ml^{-1} in 20 mM Na-HEPES, 2.0 mM DTT, 0.1 M NaCl, 10% glycerol, pH 7.0) was mixed with reservoir (0.2 M ammonium acetate, 0.1 M sodium citrate, 30% w/v PEG 4000) at a 3 μl : 2 μl protein solution : reservoir ratio and allowed to stand at room temperature. A crystallization droplet setup in the same way but with 2% (v/v) methyl-pyrrolidinone (MeP) added to the reservoir produced no crystals. A microcrystal was then transferred to this second drop and this seed crystal grew over 10 days to a size of 0.4 mm × 0.3 mm × 0.25 mm.

The autoproteolyzed active form Csp7 was inhibited by titrating Ac-DEVD-CHO into the protein sample. The complex was further purified by size-exclusion chromatography. Pooled fractions were concentrated to about 5 mg/ml for crystallization. Slow vapor diffusion was used to obtain X-ray quality crystals of the Csp7–Ac-DEVD-CHO complex over a few weeks at 4°C.

Csp8 was titrated with Ac-DEVD-CHO (12.0 mg/ml, 20 mM HEPES pH 7.0, 0.1 M NaCl, 5.0 mM β-ME) and was subsequently added to a reservoir solution (0.1 M potassium phosphate, pH 6.0, 5% *t*-butanol, 40% (w/v) ammonium sulfate) at 2 μl : 2 μl ratio and suspended over 1.0 ml of reservoir at room temperature. A single crystal was harvested within two weeks and has dimensions of 0.40 × 0.20 × 0.10 mm. The same crystal was flash cooled to 170 K in a nitrogen gas stream prior to data collection.

Data collection, structural solution and refinement

Crystals of Csp1–Ac-DEVD-CHO and Csp3–Ac-DEVD-CHO were mounted in glass capillaries for X-ray data collection at −7°C and −4°C, respectively. X-ray data of both Csp1–Ac-DEVD-CHO and Csp3 complexes were collected on an Raxis IIC image plate equipped with Rigaku rotating anode generator and processed using software provided by the manufacturers (Molecular Structures Corp., Woodlands, TX). R-merge for the data was 6.1%. at 2.2 Å resolution. Analysis of the unit cell dimensions suggested that each asymmetric unit contained two Csp3 heterodimers. A polyalanine model of a single Csp1 heterodimer was used to obtain a successful rotation and translation function solution for a Csp3 heterodimer using the program AMoRe [42]. The first solution was then fixed while a second polyalanine model was tried in the rotation and translation function. Combining the two solutions produced a polyalanine model for the Csp3 dimer of heterodimers with an R-factor of 45.1% for all observed reflections between 8 and 2.8 Å resolution, and an R-free of 47.5% for 10% of the reflections set aside at the start of the refinement. The resolution of the maps and model was gradually increased to 2.2 Å resolution by cycles of model building, positional refinement and thermal factor refinement, interspersed with torsional dynamics runs. All model refinement was carried out using the X-PLOR [43] suite of programs.

Crystals of the Csp7–Ac-DEVD-CHO complex were transferred to cryoprotectant and flash-cooled to 100K in nitrogen gas stream prior to data collection. The diffraction images were recorded on charge-coupled device (CCD) 2X2K detector at Brookhaven National Laboratories (BNL, Brookhaven, NY). The data were processed using DENZO and SCALPACK software [44]. The crystals have unit cell dimensions of 88.2 Å, 88.2 Å, 186.2 Å, $\alpha = 90.0°$, $\beta = 90.0°$, $\gamma = 120.0°$, and belong to space group P_3221. Assuming that there is one tetramer in the asymmetric unit, the calculated Matthew's specific volume was 2.6 $Å^3$/d. The structure was solved by molecular replacement methods using a truncated Csp3 tetramer molecule as the searching template. The initial R-factor and correlation coefficient factors are 44% and 65%, respectively. A polyalanine model from the solution was first refined against data between 8.0 Å and 3.0 Å. The sidechains of individual amino acids were modeled into the electron density map according to the protein sequence. The model was refined using X-PLOR and manually corrected using QUANTA (QUANTA97, Molecular Simulations, Inc). The final model has a full tetramer assembly of 654 residues, two sulfate anions and 374 water molecules.

A single crystal of Csp8–Ac-DEVD-CHO complex was flash-cooled in a nitrogen gas stream prior to the synchrotron data collection at BNL. Data was recorded on a 2X2K CCD image plate mounted on X25 beam line. The space group of the crystal was determined as C2221 with unit cell dimensions of 62.12 Å, 344.33 Å, 190.99 Å, $\alpha = 90.0$, $\beta = 90.0$, $\gamma = 90.0$. The Matthew's specific volume calculation [45] suggested that there are three independent tetrameric molecules in the asymmetric unit giving a calculated solvent content of 54%. The crystal diffracts anisotropically along the a*, b*, and c* axes to 2.35 Å, 2.80 Å and 2.65 Å, respectively. The data set was processed using DENZO and SCALPACK software to a resolution of 2.65 Å. The structure solution was obtained by using AMoRe and using a truncated Csp3 tetramer molecule as searching template. Rigid-body and positional refinement of the polyalanine model was initially carried out using X-PLOR. The sidechains, insertions and deletions of the molecule were modeled into the electron density map manually using QUANTA programs. The final model contains 1454 amino acids, 316 solvent molecules and six Ac-DEVD-CHO compounds covalently attached to the active site cysteine residue.

Accession numbers

The coordinates of the Csp-7–Ac-DEVD-CHO structure have been deposited with the Protein Data Bank under the accession code 1F1J.

Acknowledgements

We thank Vicki Sato and Thierry Hercend for reading the manuscript and making helpful suggestions.

References

1. Cohen, G.M. (1997). Caspases: the executioners of apoptosis. *Biochem. J.* **326**, 1-16.
2. Miller, D.K. (1997). The role of the Caspase family of cysteine proteases in apoptosis. *Sem. Immunol.* **9**, 35-49.
3. Nunez, G.B., Benedict, M. A., Hu, Y. & Inohara, N. (1998). Caspases: the proteases of the apoptotic pathway. *Oncogene* **17**, 3237-3245.
4. Stennicke, H.R. & Salvesen, G.S. (1998). Properties of the caspases. *Biochim. Biophys. Acta* **1387**, 17-31.
5. Thornberry, N.A. (1998). Caspases: key mediators of apoptosis. *Chem. Biol.* **5**, R97-R103.
6. Thornberry, N.A. & Lazebnik, Y. (1998). Caspases: enemies within. *Science* **281**, 1312-1316.
7. Garcia-Calvo, M., Peterson, E.P., Leiting, B., Ruel, R., Nicholson, D.W. & Thornberry, N.A. (1998). Inhibition of human caspases by peptide-based and macromolecular inhibitors. *J. Biol. Chem.* **273**, 32608-32613.
8. Ku, G., Faust, T., Lauffer, L.L., Livingston, D.J. & Harding, M.W. (1996). Interleukin-1β converting enzyme inhibition blocks progression of type II collagen-induced arthritis in mice. *Cytokine* **8**, 377-386.
9. Yaoita, H., Ogawa, K., Maehara, K. & Maruyama, Y. (1998). Attenuation of ischemia/reperfusion injury in rats by a caspase inhibitor. *Circulation* **97**, 276-281.
10. Cheng, Y., *et al*., & Holtzman, D.M. (1998). Caspase inhibitor affords neuroprotection with delayed administration in a rat model of neonatal hypoxic-ischemic brain injury. *J. Clin. Invest.* **101**, 1992-1999.
11. Endres, M., *et al*., & Moskowitz, M.A. (1998). Attenuation of delayed neuronal death after mild focal ischemia in mice by inhibition of the caspase family. *J. Cerebr. Blood Flow Metabol.* **18**, 238-247.
12. Yakovlev, A.G., Knoblach, S.M., Fan, L., Fox, G.B., Goodnight, R. & Faden, A.I. (1997). Activation of CPP32-like caspases contributes to neuronal apoptosis and neurological dysfunction after traumatic brain injury. *J. Neurosci.* **17**, 7415-7424.
13. Rodriguez, I., Matsuura, K., Ody, C., Nagata, S. & Vassalli, P. (1996). Systemic injection of a tripeptide inhibits the intracellular activation of CPP32-like proteases *in vivo* and fully protects mice against fas-mediated fulminant liver destruction and death. *J. Exp. Med.* **184**, 2067-2072.
14. Giegel, D.A. & Kostlan, C.R. (1998). Blocking interleukin-1 action. In *Annual Reports in Medicinal Chemistry* (Bristol, J.A., ed.), pp. 183-192, Academic Press, San Diego.
15. Walker, N.P.C., *et al*., & Hammill, L.D.(1994). Crystal structure of the cysteine protease interleukin-1β-converting enzyme: a (p20/p10)2 homodimer. *Cell* **78**, 343-352.
16. Wilson, K.P., *et al*., & Livingston, D.J. (1994). Structure and mechanism of interleukin-1β converting enzyme. *Nature* **370**, 270-275.
17. Margolin, N., *et al*., & Livingston, D.J. (1997). Substrate and inhibitor specificity of interleukin-1β-converting enzyme and related caspases. *J. Biol. Chem.* **272**, 7223-7228.
18. Okamoto, Y. *et al*., & Isomura, Y. (1999). Peptide based-interleukin-1β converting enzyme (ICE) inhibitors: synthesis, structure activity relationships and crystallographic study of the ICE-inhibitor complex. *Chem. Pharmaceut. Bull.* **47**, 11-21.
19. Rotonda, J., *et al.,* & Becker, J.W.(1996). The three-dimensional structure of apopain/CPP32, a key mediator of apoptosis. *Nat. Struct. Biol.* **3**, 619-625.
20. Mittl, P.R.E., *et al*., & Grütter, M.G. (1997). Structure of recombinant human CPP32 in complex with the tetrapeptide acetyl-Asp–Val–Ala–Asp fluoromethyl ketone. *J. Biol. Chem.* **272**, 6539-6547.
21. Blanchard, H., *et al*., & Grütter, M.G. (1999). The three-dimensional structure of caspase-8: an initiator enzyme in apoptosis. *Structure* **7**, 1125-1133.
22. Watt, W., Koeplinger, K.A., Mildner, A.M., Heinrikson, R.L., Tomasselli, A.G. & Watenpaugh, K.D. (1999). The atomic-resolution structure of human caspase-8, a key activator of apoptosis. *Structure* **7**, 1135-1143.
23. Laskowski, R.A., MacArthur, M.W., Moss, D.S. & Thornton, J.M. (1993). PROCHECK: a program to check the stereochemical quality of protein structures. *J. Appl. Crystallogr.* **26**, 283-291.
24. Richardson, J.S. (1981). The anatomy and taxonomy of protein structure. *Adv. Protein Chem.* **34**, 167-338.
25. Ollis, D.L. *et al*., & Remington, S.J. (1992). The α/β hydrolase fold. *Protein Eng.* **5**, 599-611.
26. Thornberry, N.A., *et al*., & Nicholson, D.W. (1997). A combinatorial approach defines specificities of members of the caspase family and granzyme B. Functional relationships established for key mediators of apoptosis. *J. Biol. Chem.* **272**, 17907-17911.
27. Golec, J.M.C., *et al*., & Livingston, D.J. (1997). Structure-based design of non-peptidic pyridone aldehydes as inhibitors of interleukin-1β converting enzyme. *Bioorg. Med. Chem. Lett.* **7**, 2181-2186.
28. Dao-Pin, S., Nicholson, H., Baase, W.A., Zhang, X.J., Wozniak, J.A. & Matthews, B.W. (1991). Structural and genetic analysis of electrostatic and other interactions in bacteriophage T4 lysozyme. *Ciba Found. Symp.* **161**, 52-62.
29. Wu, J.C. & Fritz, L.C. (1999). Irreversible caspase inhibitors: tools for studying apoptosis. *Methods* **17**, 320-328.
30. Chandler, J.M., Cohen, G.M. & MacFarlane, M. (1998). Different subcellular distribution of caspase-3 and caspase-7 following Fas-induced apoptosis in mouse liver. *J. Biol. Chem.* **273**, 10815-10818.
31. Machleidt, T., Geller, P., Schwandner, R., Scherer, G. & Kronke, M. (1998). Caspase 7-induced cleavage of kinectin in apoptotic cells. *Fed. Eur. Biochem. Studies* **436**, 51-54.
32. Saudou, F., Finkbeiner, S., Devys, D. & Greenberg, M.E. (1998). Huntingtin acts in the nucleus to induce apoptosis but death does not correlate with the formation of intranuclear inclusions. *Cell* **95**, 55-66.
33. Wellington, C.L., *et al*., & Hayden, M.R. (1998). Caspase cleavage of gene products associated with triplet expansion disorders generates truncated fragments containing the polyglutamine tract. *J. Biol. Chem.* **273**, 9158-9167.
34. Dodel, R.C., Du, Y., Bales, K.R., Ling, Z., Carvey, P.M. & Paul, S.M. (1999). Caspase-3-like proteases and 6-hydroxydopamine induced neuronal cell death. *Mol. Brain Res.* **64**, 141-148.
35. Gervais, F.G., *et al*., & Nicholson, D.W. (1999). Involvement of Caspases in proteolytic cleavage of Alzheimer's amyloid-β precursor protein and amyloidogenic Aβ peptide formation. *Cell* **97**, 395-406.
36. Ona, V.O., *et al*., & Friedlander, R.M. (1999). Inhibition of caspase-1 slows disease progression in a mouse model of Huntington's disease. *Nature* **399**, 263-267.
37. Shimohama, S., Tanino, H. & Fujimoto, S. (1999). Changes in caspase expression in Alzheimer's disease: comparison with development and aging. *Biochem. Biophys. Res. Commun.* **256**, 381-384.
38. Thornberry, N.A. *et al*., & Aunins, J.(1992). A novel heterodimeric cysteine protease is required for interleukin-1β processing in monocytes. *Nature* **356**, 768-774.
39. Gu, Y., Sarnecki, C., Fleming, M.A., Lippke, J.A., Bleackley, R.C. & Su, M.S.-S. (1996). Processing and activation of CMH-1 by granzyme B. *J. Biol. Chem.* **271**, 10816-10820.
40. Lippke, J.A., Gu, Y., Sarnecki, C., Caron, P.R. & Su, M.S.-S. (1996). Identification and characterization of CPP32/Mch2 homolog 1, a novel cysteine protease similar to CPP32. *J. Biol. Chem.* **271**, 1825-1828.
41. Chen, W., Raybuck, S.A., Fulghum, J.R., Petrillo, R.A., Margolin, N. & Chambers, S.P. (1997). Expression and purification of human interleukin-1β converting enzyme form Trichoplusia in insect cells using a baculovirus expression system. *Protein Expr. Purif.* **9**, 69-75.
42. Navaza, J. (1994). AMoRe: an automated package for molecular replacement. *Acta Crystallogr. A* **50**, 157-163.
43. Brunger, A. (1996). *X-PLOR, A System for X-ray Crystallography and NMR*. Yale University Press, New Haven.
44. Otwinowski, Z. & Minor, W. (1997). Processing of X-ray diffraction data collected in oscillation mode. *Methods Enzymol.* **276**, 307-326.
45. Matthews, B.W. (1968). Solvent content of protein crystals. *J. Mol. Biol.* **33**, 491-497.
46. Carson, M. (1991). Ribbons 2.0. *J. Appl. Cryst.* **24**, 958-961.
47. Lambert, M.H. (1997). Docking conformationally flexible molecules into protein binding sites. In *Practical Applications of Computer-Aided Drug Design*. (Charifson, P.S., ed.), pp. 243-303, Dekker, New York.
48. Nicholls, A., Sharp, K.A. & Honig, B. (1991). Protein folding and association: insights from the interfacial and thermodynamic properties of hydrocarbons. *Proteins* **11**, 281-296.